

Mechanics of Carbon Nanotubes

A Review of Basic Models and New Nanoscale Effects

Vasyl Harik

Abstract This chapter reviews basic models and new effects in the still emerging field of *Nanoscale Mechanics* and one of its essential parts: *Mechanics of Carbon Nanotubes*. Experiments with carbon nanotubes, theoretical models and modeling (i.e., molecular dynamics simulations), classification of carbon nanotubes into *four classes* (i.e., *thin and thick lattice shells, long high-aspect-ratio nanotubes and beam-like carbon nanotube crystals of small radii*) have been reviewed. Classification of carbon nanotubes is important for the safety of nanotechnology and evaluation of health effects. Interfacial sliding of the adjacent lattice shells in the multi wall carbon nanotubes (MWNT) has been discussed along with a nanoscale analog of the Newton's friction law and *the effect of spatial exclusion of electrons (ESEE)* at the interface, which effectively can be viewed as a nanoscale analog of the *Pauli's exclusion principle*. Examples of lattice waves, i.e., *phonons*, in carbon nanotubes have been presented. Ranges of applicability of estimates for the effective thickness of carbon nanotubes varying between 0.66 and 3.4 Å have been examined along with their dependence on the balance between the elastic interactions and van der Waals forces.

Dr. V. Harik, former ICASE Staff Scientist at the NASA Langley Research Center (Hampton, VA), Principal Scientist at Nanodesigns Consulting, author of a monograph and a short course entitled "*Mechanics of Carbon Nanotubes*" © (2001) presented at the Annual ASME Congress (2001 and 2004) and a co-editor of Kluwer volumes: "*Trends in Nanoscale Mechanics*" (2003) and "*Micromechanics and Nanoscale Effects*" (2004).

Nanodesigns Consulting is a 2004 spin-off from the NASA Langley Research Center, Hampton, Virginia. Its Staff consulted for the Princeton-based NASA-funded URETI Institute for Nanostructured Bio-inspired Materials (<http://bimat.org>), National Institute of Aerospace (Hampton, VA), University Space Research Association (USRA) and NASA NAIC (Atlanta).

V. Harik (✉)

Nanodesigns Consulting, P.O. Box 5303, Wilmington, DE 19808-5303, USA
e-mail: Harik@nanodesignconsult.com

A Historical Perspective

After the discovery of multiwall carbon nanotubes in 1991 by S. Iijima and single wall carbon nanotubes in 1993 by Iijima and Ichihashi of NEC laboratories in Japan [1, 2], first theoretical modeling of carbon nanotubes and carbon nanotube crystals was carried out at the IBM Watson Research Center in 1993 [3, 4]. First vibration experiments with carbon nanotubes were carried out in 1996 [5, 6] at the time of first molecular dynamics (MD) simulations of buckling of carbon nanotubes [7, 8]. The nomenclature for the physical description of carbon nanotubes and their chirality (e.g., armchair and zig-zag) has been proposed in 1992 [9]. Classification of carbon nanotubes into four classes¹ of *thin and thick lattice shells, long high-aspect-ratio nanotubes and beam-like carbon nanotube crystals of small radii* (Fig. 1) has been developed in 2001 [10, 11]² at the NASA Langley Research Center in Hampton, Virginia.³

Length Scales in the Structure of Carbon Nanotubes

The atomic structure of carbon nanotubes (C_{NT}) consists of six carbon atoms arranged in hexagonal carbon rings (Fig. 2). The key length-scale parameters that describe the atomic structure of C_{NT} lattices include the length of the covalent σ -bond, l_{C-C} , 1.41–1.44 Å, the size of a carbon ring, $a = 2.46$ Å, the radius, R_{NT} , of C_{NT} lattices (~ 0.2 –2 nm, for the single wall nanotubes, and ~ 35 nm for the multi wall nanotubes) or the diameter, d_{NT} , and their length, L_{NT} , varying between few nanometers and 100 s of microns (even a few centimeters).

The length scale associated with the length of the C–C bond, l_{C-C} , is important for the evaluation of relative deformation of C–C bonds in the elastic interactions, dynamics vibrations and structural deformations, as well as for the scaling analysis of the energy distribution of covalent electrons and the out-of-plane π -electrons [12]. The C–C bonds can be stretched from its minimum size of 1.41 Å in the graphene sheets to longer lengths of about 1.62 Å in the carbon nanotubes of smaller radii [12]. The length scale associated with the size of a carbon ring, a , is

¹ Classification of new types of materials is important in any field of science, especially, for the highly promising carbon nanotubes, which can be separated into four distinct classes associated with quite distinct geometric parameters and some similarities with *asbestos* though.

² This research results have been first published at NASA and its ICASE Institute; see Harik, V.M., 2001. *Ranges of applicability for the continuum-beam model in the constitutive analysis of carbon nanotubes: nanotubes or nano-beams?* (NASA/CR-2001-211013, NASA Langley Research Center), Hampton, Virginia, USA. Harik, V.M., 2001. *Mechanics of carbon nanotubes* © 2001. ASME Education Institute (Notes for a Short Course, a 2002 CD and a 2001 video), American Society of Mechanical Engineers, New York, NY.

³ For more historical perspectives and some epistemological notes about the concepts of emerging *Nanoscale Mechanics* see author's footnotes for the references cited in this chapter.

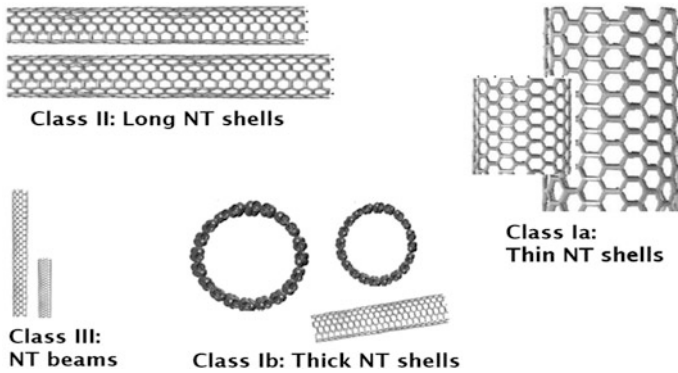


Fig. 1 Classification of carbon nanotubes (NT or C_{NT}) into four classes (after [12]): the thin C_{NT} shells (Class Ia), the thick C_{NT} shells (Class Ib), the long C_{NT} shells (Class II, i.e., the high aspect ratio C_{NT} shells) and the C_{NT} nano-beams and C_{NT} nanocrystals (Class III)

essential for nanoscale homogenization⁴ [11, 12] and analysis of relative deformation of graphene sheets (Fig. 2) and segments of carbon nanotubes (Fig. 3 and Table 1).

The diameter-to-length aspect ratio, d_{NT}/L_{NT} , of the carbon nanotube lattice (Fig. 3) is an important structural parameter in many applications such as in the nanotube based AFM probes and in the buckling process of C_{NT} lattices [10–12]. The ratio of the radius, R_{NT} , to the carbon ring size, a , i.e., R_{NT}/a , or the normalized circumference, $2\pi R_{NT}/a$, are important in the evaluation of radial deformation of carbon nanotubes and the radial buckling of C_{NT} lattices [7–11]. Separation and collapse of the adjacent length scales result in different classes of C_{NT} lattices (Fig. 1): *thin nanotubes*, *thick nanotubes*, *nano-beams of small radii* and the *high aspect ratio nanotubes* [10–12].

Nanoscale Homogenization Criterion

The material properties of different classes of carbon nanotubes and their C_{NT} lattices become unique and independent of their size or the number of atomic unit layers shown in Fig. 3, for instance, when the C_{NT} atomic structure satisfies a nanoscale criterion for the unique averaging (or *homogenization*) of the material properties over a nanoscale volume or an extended surface:

⁴ Nanoscale homogenization itself and nanoscale homogenization criteria [11, 12], in particular, are very important for the application of continuum concepts (e.g., continuous surface or a properly-defined number of representative volume elements for the volume-averaging for the uniquely-defined material properties of any material having a discrete atomic lattice structure) to the C_{NT} lattice structures (for more details, see the next part of this chapter).

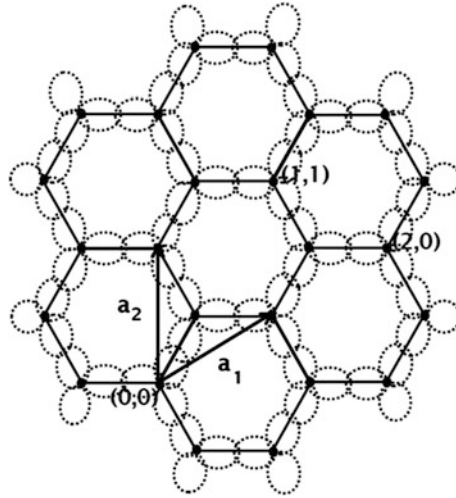


Fig. 2 Atomic lattice structure of a graphene flake (Nanoscale mechanics of graphene sheets and flakes has been presented in Ref. [12], which includes a chapter on electronic energy barriers in graphene, deformed Fermi cones, material and mechanical properties, interfacial sliding and nanoscale friction, lattice waves, i.e., *phonons*, etc.) and that of carbon nanotubes with the hexagonal carbon rings of carbon atoms and a schematic of the electron distribution in the C–C bonds. The (n, m) lattice structure is based on the unit vectors a_1 and a_2

Fig. 3 Schematic of a carbon ring with the length of the C–C bond, $l_{C-C} = 1.41\text{--}1.42 \text{ \AA}$, and the size of 2.46 \AA , and the atomic lattice structure of an armchair $(10, 10)$ carbon nanotube of diameter, $d_{NT} = 13.6 \text{ \AA}$, and the length, $L_{NT} = 52.5 \text{ \AA}$, which represent the four length scales involved

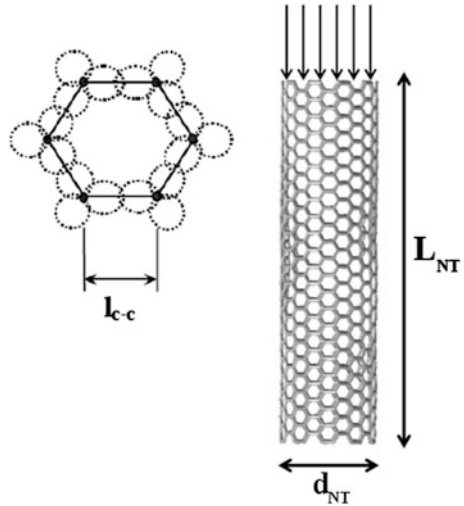


Table 1 The length scales in the structure of single wall carbon nanotubes

Parameters	Typical values	Ranges of values ^a
C–C bond length, l_{C-C}	1.41–1.42 Å	1.41–1.62 Å
Carbon ring size, a	2.46 Å	~2.22–2.70 Å
Effective thickness, h_{NT}	0.66–3.4 Å	Load path dependent
Diameter, d_{NT}	~1 nm	4–50 Å
Length, L_{NT}	~20–100 nm	Vary in AFM/NEMS
Length, L_{NT}	100 nm–1 μm–3 cm	Vary in nanocomposites

^a Ranges of values of the C–C bond length, l_{C-C} are associated with the bond stretching in the C_{NT} lattices of small radii. The carbon ring size, a , may vary under the tensile and compressive loading and the C_{NT} lattice corrugation. The effective thickness, h_{NT} , depends on the type of loads and the load path through thermodynamic states of the deformation process (for details see [12])

$$L_{NT} \gg a, \quad (1)$$

or $L_{NT}/a \gg 1$, where the length of a C_{NT} lattice, L_{NT} , should be considerably greater than the size of a carbon ring, $a = 2.46$ Å, its smallest structural element [10–12]. The inequality in the homogenization criterion (1) means roughly an order of magnitude difference, i.e., $L_{NT}/a \approx 10$. It turns out that the molecular structure of the fullerene C60, i.e., the Buckminster buckyball with $a \approx 2.46$ Å, represents the smallest stable nanostructure [12], the surface of which satisfies the aforementioned homogenization criterion (1) due to Harik [10–12].

Classification of Carbon Nanotubes

Carbon nanotubes with large values of radius, R_{NT} , have small curvature, i.e., $1/R_{NT} \ll 1$, and atomic lattices with elastic properties similar to the graphene sheets [12]. This class of *thin C_{NT} lattice shells* (Fig. 1) satisfies, the following criterion for the ratio of the effective thickness, h_{NT} , of C_{NT} lattices to their radius, R_{NT} : $h_{NT}/R_{NT} \ll 1$ [10, 11]. The two adjacent length scales: R_{NT} and the effective thickness, h_{NT} (or the bond length, l_{C-C}) are well separated, and the bond length, l_{C-C} , plays virtually no role in the global deformation response for small strains.

Deformation of single wall carbon nanotubes having large values of radius, $R_{NT} = \frac{a}{2\pi} \sqrt{n^2 + m^2 + nm}$, can depend on their chirality defined by the (n, m) pair and the following scaling condition for the class of *thin C_{NT} lattices* (Fig. 1):

$$h_{NT} \ll \frac{a}{2\pi} \sqrt{n^2 + m^2 + nm} \quad (2a)$$

or

$$\frac{h_{NT}}{R_{NT}} = \frac{2\pi h_{NT}}{l_{C-C}\sqrt{3(n^2 + m^2 + nm)}} \ll 1. \quad (2b)$$

The advantage of this form is evident when single carbon rings are deformed in the (n, m) C_{NT} lattices, and the nanoscale homogenization criterion (1) for the carbon rings is more difficult to apply. Carbon nanotubes satisfying the scaling conditions (2a, b) deform as thin lattice shells.

Since the effective C_{NT} thickness, h_{NT} , can be estimated as a half of the C–C bond length, 0.72 Å [10–12], the presence of the carbon ring size, a , the effective C_{NT} thickness, h_{NT} , and the C–C bond length, l_{C-C} , in the new thin lattice-shell conditions (2a, b) can be avoided by presenting them in the following form, which is solely based on the (n, m) nomenclature for the C_{NT} lattices:

$$\frac{\pi}{\sqrt{3(n^2 + m^2 + nm)}} \ll 1 \quad (3)$$

The (10, 10) C_{NT} lattice ($R_{NT} = 6.8$ Å, Fig. 3) satisfies the thin lattice-shell conditions (2a, b) and (3). It so happens that the (10, 10) C_{NT} lattice shown in Fig. 3 is the smallest armchair nanotube, which fulfills this condition for the class of *thin C_{NT} shells* [10–12]. The C_{NT} lattices of larger radii (both with the armchair and the zig-zag chirality) also satisfy the conditions (2a, 2b) and (3). The class of *thick C_{NT} lattices* [10–12] satisfies, a related condition for the radius, R_{NT} , of carbon nanotubes and the effective C_{NT} thickness, h_{NT} (see Table 2):

Table 2 Values of the effective C_{NT} lattice thickness, h_{NT} estimates for carbon nanotubes

Types of analysis used in nanoscale analysis	C _{NT} thickness estimates, h_{NT} Å	Authors of the C _{NT} thickness estimates
Molecular dynamics (MD) simulations	0.66	Yakobson et al. [7, 8]
Scaling analysis ^a of bonds in carbon rings	0.71–72	Harik [11, 12]
Tight-binding method (atomic scale)	0.74	Zhou et al. [13]
Local density approximation	0.75	Tu and Ou-Yang [14]
Continuum shell theory	0.75	Panatano et al. [15]
Ab initio computations	0.665	Wang et al. [16]
Continuum ring theory	0.617	Vodenitcharova and Zhang [20]
Atomic potential based analysis	0.62–0.87	Huang et al. [80]
Continuum modeling	0.87	Goupalov [21]
Ab initio computations	0.89	Kudin et al. [17]
Continuum hollow cylinder	0.98	Sears and Batra [22, 23, 34]
C _{NT} bundle-based crystal	3.42	Tersoff and Ruoff [4]
Molecular dynamics (MD) simulations	~ 3.4	Avouris et al. [18]

^a The effective C_{NT} lattice thickness, h_{NT} can be estimated as a half of the length of the C–C bonds, $l_{C-C} = 1.41$ – 1.44 Å via a spherical approximation for the distribution of σ -electrons in the elastic load-transferring bonds [10–12]

$$\frac{h_{NT}}{R_{NT}} = \frac{2\pi h_{NT}}{a\sqrt{n^2 + m^2 + nm}} > 1/10 \quad (4)$$

Carbon nanotubes of small radii $R_{NT} < 6 \text{ \AA}$ or $R_{NT}/a < 2$, satisfy this condition for the class of *thick* C_{NT} lattices. These radii are close to the radii of C_{NT} *nano-beams* [12], which have smaller number of the circumscribed carbon rings along their circumference and much greater curvature (Fig. 1). Long high-aspect-ratio carbon nanotubes (class II, Fig. 1) have C_{NT} *lattice shells* of the length, L_{NT} , such that $d_{NT}/L_{NT} < 1/10$, and considerable surface with the surface effects proportional to their surface area: $\pi d_{NT} L_{NT}$ or $a\sqrt{n^2 + m^2 + nm} L_{NT}$.

The length scale and the size effects associated with the C_{NT} lattice length, L_{NT} , which influence the global deformation of carbon nanotubes and their material properties (for short C_{NT} lattices), are represented in both the aspect ratio, d_{NT}/L_{NT} and the homogenization ratio, L_{NT}/a , or the minimum homogenization length, L_H . At the length scale level associated with the C_{NT} radius, R_{NT} , the mechanical material properties of carbon nanotubes are influenced not only by their chirality, but also by the thickness-to-radius ratio, h_{NT}/R_{NT} . For the C_{NT} nano-beams [12], the curvature effects and the degree of bond stretching are also important due the structural properties of carbon nanotubes having small radius.

Effective Thickness of Carbon Nanotubes

The value of the effective C_{NT} lattice thickness, h_{NT} , is affected by the degree of the balance the elastic C–C bond interactions associated with the approximation: $h_{NT} \approx l_{C-C}/2$ [11, 12], Table 2, and the van der Waals forces associated with the experimental graphene value of $h_{NT} \approx 3.4 \text{ \AA}$. The value of the effective lattice thickness, h_{NT} , in a particular deformation response of the C_{NT} lattice (e.g., axial buckling with $h_{NT} \approx l_{C-C}/2$, or other types of deformations with h_{NT} such that $l_{C-C}/2 < h_{NT} < 3.4 \text{ \AA}$, Fig. 3) is associated with the specific change in the potential energy, U , of the considered atomic lattice (Table 2).

In a physical setting, the balance between the elastic C–C bond interactions and the van der Waals forces in a deformation response of the C_{NT} atomic lattices associated with a particular loading path, can be described by the following approximation equation [12]:

$$\sum_{i=1}^{n_C} \frac{1}{V_{C-C,i}} \left| \left(\frac{\partial^2 U}{\partial \varepsilon^2} \right)_{\varepsilon=0,i} \right|_{C-C} = \frac{h_C}{h_0} \sum_{i=1}^{n_{vdW}} \frac{1}{V_{vdW,i}} \left| \left(\frac{\partial^2 U}{\partial \varepsilon^2} \right)_{\varepsilon=0,i} \right|_{vdW}, \quad (5)$$

where n_C is the number of carbon atoms in the C_{NT} lattice, all of which are obviously associated with the C–C bond interactions, n_{vdW} is the number of atoms affected by the van der Waals interactions because of their displacement in radial direction, and the proportionality coefficients, h_C and h_0 , characterize the discrete

and the homogenized contributions of the C–C bond interactions to the value of the effective thickness, h_{NT} , of C_{NT} lattice: $h_{NT} = h_0 h_{vdW}$, with $h_{vdW} = 3.4 \text{ \AA}$, $0 < h_0 \leq 1$, and $h_C > 1$, for most axial deformations, and $h_C = 0$ and $h_0 \approx 1$, for the C_{NT} lattices with large diameters subjected to the predominately surface forces proportional to the surface area of the carbon rings, N_{vdW} , under significant van der Waals forces, as in the case of graphene sheets under the transverse loading [12]:

$$h_0 = \frac{1}{2} l_{C-C} / h_{vdW} + \frac{l_{C-C}}{2\pi R_{NT}} \frac{\frac{3}{2} a N_{vdW}}{L_{NT}} \left(1 - \frac{1}{2} l_{C-C} / h_{vdW}\right), \quad (6)$$

Note that $h_C = h_0$, when the elastic forces (i.e., the C–C bond interactions) and the van der Waals forces exactly balance each other during the deformation response of a C_{NT} lattice and the corresponding loading path.

The value of the effective thickness, h_{NT} , of C_{NT} lattice shells can be estimated by the number of carbon rings, N_{vdW} , subjected predominately to the van der Waals forces [12]:

$$h_{NT} = \frac{1}{2} l_{C-C} + \frac{l_{C-C}}{2\pi R_{NT}} \frac{3a N_{vdW}}{2L_{NT}} \left(h_{vdW} - \frac{1}{2} l_{C-C}\right), \quad (7a)$$

or by the number of carbon rings, N_{C-C} , mostly involved in the elastic C–C interactions [12]:

$$h_{NT} = h_{vdW} - \frac{l_{C-C}}{2\pi R_{NT}} \frac{3a N_{C-C}}{2L_{NT}} \left(h_{vdW} - \frac{1}{2} l_{C-C}\right). \quad (7b)$$

The value of the effective C_{NT} thickness, h_{NT} , in a particular deformation response is such that $l_{C-C}/2 \leq h_{NT} < 3.4 \text{ \AA}$ [12].

Deformation of Carbon Nanotubes

Since the discovery of carbon nanotubes in 1991 by S. Iijima and his NEC lab [1, 2], the mechanical response of single wall nanotubes (SWNT) had been evaluated via atomistic and molecular dynamics (MD) simulations [3, 4, 7, 12–19] and experimental testing [5, 6]. In these studies, the multi-cylinder crystal model [4], the continuum shell theory [7, 8, 11, 12, 15, 17, 20–25] and the continuum beam model [5, 6, 10–12] were used to examine the mechanical deformation of carbon nanotubes and deduce their Young's modulus (Table 3).

In 1999, Govindjee and Sackman [25] had considered an elastic multi-sheet model to show the explicit dependence of material properties on the system size when a continuum cross-section assumption is made for a multi-shell system subjected to bending. The continuum assumption was shown to hold when more than 201 shells are present in the macromechanical system considered. In 2001, it

Table 3 Young’s modulus of single wall carbon nanotubes in early experiments

Methods used in a study	Predicted values	Authors of predictions
Molecular dynamics (MD)	5.5 TPa ^a	Yakobson et al. [7, 8]
AFM (Fig. 5) vibration experiments	1.5–5 TPa	Treacy et al. [5]
AFM bending experiments	1.3 TPa	Wong et al. [6]
AFM tensile experiments	0.32–1.5 TPa	Yu et al. [81]

^a Molecular Dynamics (MD) predictions [7, 8] of Young’s modulus are associated with the value of 0.66 Å for the effective thickness, h_{NT} , of carbon nanotubes

was shown that nanoscale scaling analysis and the length scales associated with the geometric parameters of C_{NT} atomic lattice structure can define a set of restrictions on the assumptions that are used in the Euler beam model [10, 11].

Ru [24] proposed an intrinsic bending stiffness for carbon nanotubes in order to decouple the bending C_{NT} shell stiffness from their ill-defined effective thickness, h_{NT} , and to ensure a consistent use of the classical shell theory [26]. Soon after it was shown [10, 11] that the thickness of carbon nanotubes may have no direct effect on the buckling behavior of C_{NT} atomic lattices for two classes of C_{NT} structures (e. g., C_{NT} nanocrystals or C_{NT} nano-beams, Fig. 1) and most continuum models are applicable only within a certain range of the length scale parameters.

Extensive atomistic and MD simulations of carbon nanotubes remain computationally expensive. As a result, the continuum models that are appropriately tailored for a particular molecular structure and specific loading conditions may be useful for the qualitative analysis of constitutive behavior of carbon nanotube lattice shells. Since the mechanics of C_{NT} response is likely to depend on the C_{NT} lattice structure, a blend of nanoscale scaling analysis [10, 11] and the continuum mechanics models based on atomic potentials [27–29], whenever possible, seems appropriate for the development of a methodology for the inter-scale extension of continuum models to the nanoscale level for various nanostructures including carbon nanotubes and for optimization of the nanotube-based AFM probes for the atomic force microscopy [12]. It has been shown [10–12] that each theoretical and experimental prediction for the most types of C_{NT} deformation can be extended to a full class of carbon nanotubes (Fig. 1) through *the laws of similitude*.

Axial Buckling of Carbon Nanotubes

Axial buckling of carbon nanotubes is especially important for the optimization and design of AFM probes. Yakobson et al. [7, 8] presented molecular dynamics (MD) simulations of carbon nanotubes under axial buckling and demonstrated a shell-like buckling deformation response. Due to the lack of established characterization methods for the mechanical properties of such nanoscale structures, an analogy with macroscopic continuum beams and shells, which had some geometric similarities with the carbon nanotubes and their global behavior, was used. Such analogy

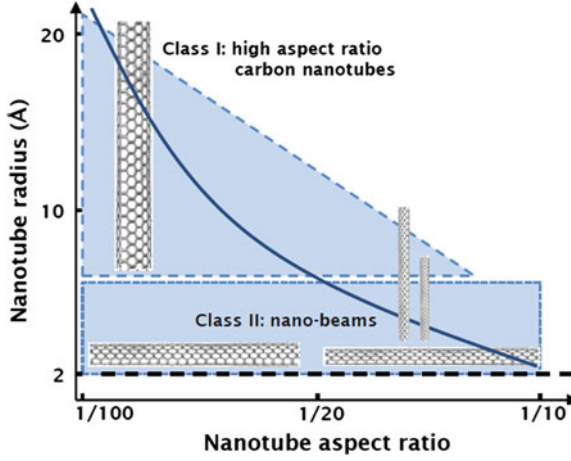


Fig. 4 A parametric map for the two classes of the high aspect ratio carbon nanotubes: *long* C_{NT} shells (class I) and the C_{NT} nanocrystals of small radii, i.e., the C_{NT} nano-beams (class II). The thick line ($\sim 1/(10d_{NT}/L_{NT})$) represents a boundary for the optimal material structure of the high aspect ratio C_{NT} lattices (after [10–12])

provided estimates for the C_{NT} Young’s modulus, E_{NT} , which may reach as high as 1,000 GPa. Such simple models provide an attractive tool for the data reduction and the analysis of structure–property relationships for nanostructured materials and carbon nanotubes, in particular.

A macromechanical model “may serve as a useful guide, but its relevance for a covalent bonded system of only a few atoms in diameter is far from obvious” [7, 8]. The MD buckling strain predictions of 0.05 % indicate hyperelastic rather than elastic behavior of C_{NT} lattice shells. To ensure the robustness of data reduction schemes that are based on continuum mechanics, a careful analysis of continuum approximations used in macromechanical models and possible limitations of this approach at the nanoscale level is required [10–12].

The aspect ratio, d_{NT}/L_{NT} , of the C_{NT} lattice structures, or its equivalent, R_{NT}/L_{NT} , is the main non-dimensional length scale parameter governing the nanoscale critical buckling (Fig. 4) and the buckling strain, ε_{cr} , of the high aspect ratio carbon nanotubes (Fig. 1):

$$\varepsilon_{cr} = 4\pi^2 \frac{R_{NT}^2}{L_{NT}^2} \left[\left(1 + \frac{h_{NT}}{2R_{NT}} \right)^2 - \left(1 - \frac{h_{NT}}{2R_{NT}} \right)^2 \right], \quad (8)$$

where h_{NT} is the equivalent thickness of the thick or thin C_{NT} lattice shells. Note that the C_{NT} buckling strain, ε_{cr} , also depends on the thickness-to-radius ratio, h_{NT}/R_{NT} , of high aspect ratio carbon nanotubes, but only in the second order effects.

The explicit dependence of the critical buckling strain, ε_{cr} , on the helicity of the atomic lattices of carbon nanotubes can be estimated by

$$\varepsilon_{cr} = 4\pi^2 \left(\frac{a\sqrt{n^2 + nm + m^2}/\pi + h_{NT}}{2L_{NT}} \right)^2 - 4\pi^2 \left(\frac{a\sqrt{n^2 + nm + m^2}/\pi - h_{NT}}{2L_{NT}} \right)^2, \quad (9a)$$

where L_{NT} is aN_a or $a\sqrt{3}N_a$ for the armchair and zig-zag carbon nanotubes, respectively; N_a is the number of carbon rings along the C_{NT} length, L_{NT} . Since the effective C_{NT} thickness, h_{NT} , can be estimated as a half of the C–C bond length, 0.72 Å [10–12], the nanoscale analog of the Euler formula (9a, b) for the critical buckling strain of the (n, m) C_{NT} lattice shell can be written as

$$\varepsilon_{cr} = 4\pi^2 \left[\left(\frac{a\sqrt{n^2 + nm + m^2}/2\pi + l_{C-C}}{4L_{NT}} \right)^2 - \left(\frac{a\sqrt{n^2 + nm + m^2}/2\pi - l_{C-C}}{4L_{NT}} \right)^2 \right], \quad (9b)$$

where the C–C bond length is about 1.41–1.62 Å, as it can be shorter or elongated. Under extensive elongation of the C–C bonds, the approximation: $h_{NT} \approx l_{C-C}/2$, has its limitations, which are also affected by the balance between the elastic C–C bond interactions and the van der Waals forces [12]. Applicability of any continuum model for carbon nanotubes has its limitations, i.e., a , the size of carbon ring.

The Model Applicability Map

Ranges of applicability of the nanoscale analogs (9a, b) of the Euler formula (8) for the axial buckling of the high aspect ratio carbon nanotubes are defined by the carbon ring size, a , on one side of the model applicability map (Fig. 4) and by the values of the C_{NT} lattice aspect ratio, i.e., the so called shell-beam transition border line $\sim 1/(10d_{NT}/L_{NT})$, beyond which geometric parameters define the class of *thin C_{NT} shells* [12]. The key non-dimensional parameters that govern the materials map for the beam-like carbon nanotubes (i.e., the class of the high aspect ratio C_{NT} lattices and the class of nano-beams, Fig. 1), include the aspect ratio, d_{NT}/L_{NT} , the homogenization ratio: L_{NT}/a , and the normalized radius, R_{NT}/a (Fig. 4) [10–12].

Examples of the atomic lattices of the C_{NT} nano-beams include [12, 30]:

- the (2, 2) C_{NT16} nanocrystals;
- the (3, 3) C_{NT24} nanocrystals;
- the (3, 0) C_{NT12} nanocrystals;
- the (4, 0) C_{NT16} nanocrystals;
- the (6, 0) C_{NT16} nanocrystals.

The atomic lattice structure of the C_{NT} nano-beams has characteristic bond stretching due to the curvature, the small radii and considerable corrugation [12, 30].

Materials maps for the class of beam-like C_{NT} nanocrystals (or the C_{NT} nano-beams) indicate that the unique material properties of the corresponding C_{NT} lattices have the mechanical properties and the associated deformation response of the beam-like structures. Ranges of applicability for the equivalent-continuum beam models [10–12, 31] span two different groups of geometric parameters (Fig. 6) that define two different classes of C_{NT} lattices with small and large values of radii (Fig. 1). It has been shown that these carbon nanotubes have the same buckling behavior [10–12], although other mechanical properties (e.g., transverse stiffness) may diverge due to different structural characteristics [12, 32, 33].

The Thin Shell Effects in the Buckling of Carbon Nanotubes

The global mechanical behavior of the carbon lattice can be analyzed by representing the discrete molecular structure with an equivalent shell [7, 8, 12, 15, 21–24, 27–29, 34]. This representation can be used to define a homogeneous equivalent-continuum⁵ by equating the energies of the two corresponding systems [7, 8]. The global shell-like response of a short C_{NT} lattice of 1 nm in diameter was first shown by Yakobson et al. [7, 8] by the molecular dynamics (MD) simulations. Equivalence between the potential energy of the C_{NT} lattice and its elastic strain energy represented by the continuum shell model [26] was used to obtain the value of the axial and flexural bending stiffness, $C = E_{NT}h_{NT} = 59.36$ eV/atom, and $D = E_{NT}(h_{NT})^3/12(1 - \nu^2) = 2.886$ eV Å²/atom. For the Poisson's ratio, ν , of 0.19, these two equations yield the Young's modulus, $E_{NT} = 5.5$ TPa, and the equivalent C_{NT} thickness, $h_{NT} = 0.66$ Å [7, 8, 32, 33]. Other authors have obtained similar values of 5.1 TPa and 0.74 Å, or 4.8 TPa and 0.75 Å (see Table 2) [12].

Carbon nanotubes of the radii $R_{NT} > 6$ Å or $R_{NT}/a > 2$, have larger radii than the C_{NT} nano-beams (Fig. 4) and the greater number of the circumscribed carbon rings along their circumference, i.e., more than 12, which corresponds to the C_{NT} lattice shells larger than the (12, 0) zig-zag carbon nanotube, e.g., the (15, 0) zig-zag C_{NT} lattice shell. Carbon nanotubes with many circumscribed carbon rings are quite different from the C_{NT} nano-beams (Fig. 1) [12]. The C_{NT} lattice shells of large diameters, $d_{NT} > 12$ Å, have much smaller intra-tubular van der Waals forces and small curvature effects. The highly-concentrated intra-tubular van der Waals forces and significant curvature effects in the C_{NT} nano-beams represent volumetric as opposed to the surface effects [4, 12].

The buckling strain, ε_{cr} , for the class of thin C_{NT} lattices (Fig. 1) having (m, n) chirality can be estimated by the following formulae for the nanoscale critical buckling strain, ε_{cr} [12]:

⁵ V.M. Harik et al. 2002. *Applicability of the Continuum-shell Theories to the Mechanics of Carbon Nanotubes*. (NASA/CR-2002-211460/ICASE Report No. 2002–2007, ICASE Institute) NASA Langley Research Center, Hampton, Virginia. In this NASA report model applicability map [12] for the continuum shell models has been presented.

$$\varepsilon_{cr} = \frac{2\pi}{\sqrt{(1-\nu^2)}} \frac{h_{NT}/a}{\sqrt{3(n^2 + m^2 + nm)}}, \quad (10a)$$

or

$$\varepsilon_{cr} = \frac{2\pi}{\sqrt{(1-\nu^2)}} \frac{h_{NT}/l_{C-C}}{\sqrt{n^2 + m^2 + nm}}, \quad (10b)$$

which represent the nanoscale analogs of the following formula: (see footnote 5)

$$\varepsilon_{cr} = \frac{1}{\sqrt{3(1-\nu^2)}} \left(\frac{h_{NT}}{R_{NT}} \right),$$

where ν is the Poisson's ratio [12] of atomic C_{NT} lattices shells (Fig. 5).

Formulae (10a, b) are valid when the nanoscale homogenization criterion (1), the scaling condition for the class of thin shells: $h_{NT}/R_{NT} \ll 1$, or the new nanoscale thin lattice-shell conditions (2a, b) and (3) for the (n, m) C_{NT} lattices are fulfilled. The role of van der Waals forces is discussed in more details in a new book *Mechanics of Carbon Nanotubes* [12]. Formulae (10a, b) and their counterparts for the nanoscale buckling provide good estimates for the axial buckling of carbon nanotubes as was shown by Harik [10–12] for different classes of atomic lattices and verified with the molecular dynamics (MD) data [12]. Each theoretical and experimental prediction is applicable and extendable within one class of carbon nanotubes [10–12] or a class of single shells in multi wall carbon nanotubes (with the role of van der Waals forces taken into account [12]).

Interfacial Sliding of Shells in Multi Wall Carbon Nanotubes

At the nanoscale level fundamental origins of sliding friction involve the surface-to-surface interactions such as the interlocking and registry effects [35–41] between the C_{NT} lattice structures (Fig. 5) and the morphology of asperity distribution, the sliding induced excitation of atomic lattice vibrations [42], interaction of phonons [43, 44] propagating along the sliding surfaces [45, 46], electrostatic interactions, electron motion and the electron interactions akin to the π – π bonding interactions [12]. These interfacial friction mechanisms have been studied to some extent by a quartz-crystal microbalance, scanning force microscopy and the nanotube pullout, AFM and TEM experiments (Fig. 6), as well as theoretical modeling including MD simulations [12].

Fig. 5 Atomic lattice of a single wall (10, 10) carbon nanotube with the C_{NT} length $L_{NT} = 52.5 \text{ \AA}$ and diameter, $d_{NT} = 13.6 \text{ \AA}$, and a schematic of a multi wall carbon nanotube (after [12])

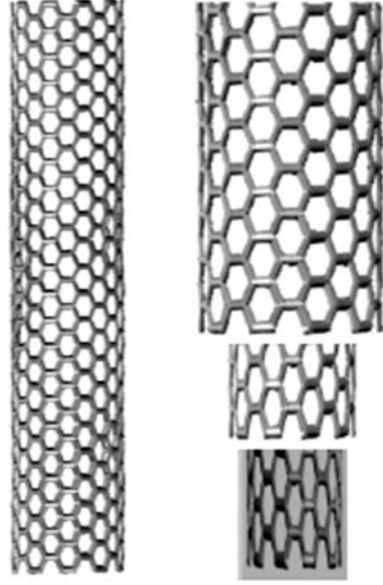
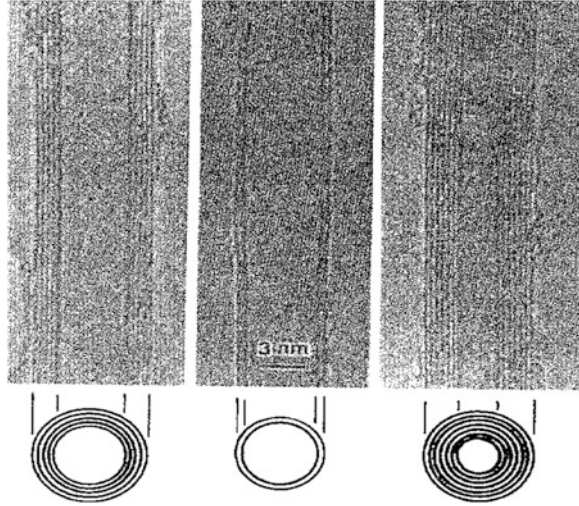


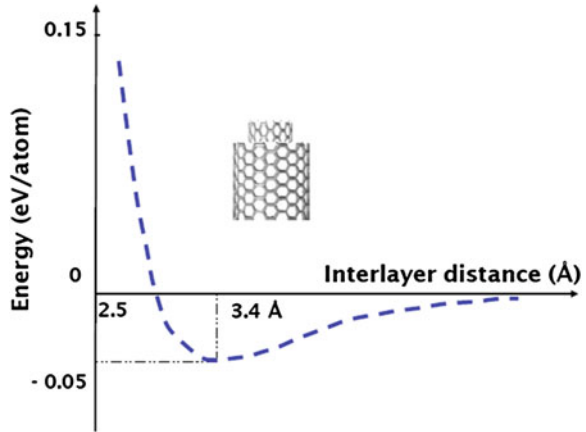
Fig. 6 TEM images of multi wall carbon nanotubes with different inner and outer diameters with five, two and seven cylindrical lattice shells reported by Iijima in 1991 (after [1])



Nanoscale Analogs of the Newton's Friction Law

Nanoscale friction between adjacent C_{NT} lattice shells in multi wall carbon nanotubes (Fig. 5) can be described at the length-scale longer than the size of carbon rings, a , by a nanoscale analog of the Newton's friction law [12, 39–41] as follows. The average shear stress, $\langle \tau_{rz} \rangle$, for planar sliding interactions can be defined as $\langle \tau_{rz} \rangle \approx \langle f \rangle_{pull} / A_{ss}$, where $\langle f \rangle_{pull}$ is the average force applied to the C_{NT} lattice and

Fig. 7 Energy of interfacial interactions due to the van der Waals forces between adjacent lattices in a multi wall carbon nanotube (with the graphene-based equilibrium distance of 3.4 Å)



A_{ss} is the common interfacial area of steady sliding between the inner and the outer C_{NT} lattices. The average strain rate, $\langle \dot{\gamma} \rangle$, can be estimated by $\langle \dot{\gamma} \rangle \approx \frac{\partial \langle V_z \rangle}{\partial r}$, where $\langle V_z \rangle$ is the average C_{NT} velocity in the axial z -direction and r is the radial distance. Then, a nanoscale analog of the Newton's law for steady C_{NT} sliding is given by [1, 12, 39–41, 47]

$$\langle \tau_{rz} \rangle = \mu_{eff} \frac{\partial \langle V_z \rangle}{\partial r}, \quad (11)$$

where μ_{eff} is an effective viscosity for the C_{NT}/C_{NT} interfacial sliding and the strain rate can be approximated as $\frac{\partial \langle V_z \rangle}{\partial r} \approx \frac{\langle V_z \rangle}{h_{vdW}}$ with the change in sliding velocity across the interfacial separation, h_{vdW} , estimated as the average C_{NT} velocity, $\langle V_z \rangle$. The average surface separation, h_{vdW} , is caused by the van der Waals forces, which can be described by the Lennard-Jones potential:

$$U_{LJ}(r) = \varepsilon \left(\frac{r_0^2}{r^{12}} - \frac{r_0^2}{r^6} \right),$$

where ε is the depth of the potential well and r_0 is the distance between two C_{NT} lattices at which the potential, U_{LJ} , is zero (Fig. 7).

In order to complete the description of the interface model, the effective viscosity, μ_{eff} , should be described. The C_{NT} velocity, $\langle V_{NT} \rangle = \langle V_z \rangle$, is, on average, linearly related to the average applied force, $\langle f \rangle$ [39–41], and the slope, χ_{eff} , can be determined. The resulting force-velocity dependence: $\langle f \rangle = \chi_{eff} \langle V_{NT} \rangle$ is a nanoscale analog of the friction law in equation (11). Then, the complete interfacial friction model [12, 39–41] for the sliding process is given by

$$\langle f \rangle_{pull} = f_0 + \chi_{eff} \langle V_{NT} \rangle, \quad (12)$$

where f_0 is the critical force associated with the onset of interfacial sliding of the inner carbon nanotube [12, 39–41].

The applied force, $\langle f \rangle$, is related to the shear stress in Eq. (11) by the force balance: $\langle f \rangle = \langle \tau_{rz} \rangle A_{ss}$. Therefore, the viscosity coefficient, χ_{eff} , can be related to the effective viscosity μ_{eff} by

$$\mu_{eff} = \chi_{eff} \frac{h_{vdW}}{R_{NT}} \left[2\pi \left(1 + \frac{h_{NT}}{2R_{NT}} \right) L_{NT} \right]^{-1} \quad (13)$$

and the complete interfacial friction model (12) takes the following form [12]:

$$\langle f \rangle_{pull} = f_0 + 2\pi\mu_{eff} \left[\frac{h_{vdW}}{R_{NT}} \right]^{-1} \left(1 + \frac{h_{NT}}{2R_{NT}} \right) L_{NT} \langle V_{NT} \rangle, \quad (14)$$

The magnitude of the critical force f_0 is on order of *pico-Newtons*, the value of coefficient χ_{eff} may vary in the range of (pN ps)/Å units and the average C_{NT} velocity, $\langle V_z \rangle$, is on order of Å/ps or 100 s of m/s at the nanoscale level. The effective viscosity μ_{eff} , which characterizes the viscosity of the spatially distributed π -electrons, is associated with the transient interlocking of π -electrons in the spatial energy map shown on Fig. 8b for a quasi-static case. The viscosity of π -electrons is on the order of fractions of centi-Poise for the noted range of velocities [12].

Effect of the Spatial Exclusion of Electrons (SEE)

Variations in the interfacial frictional forces and the picosecond spikes in the axial velocity, V_{NT} , of a sliding carbon nanotube lattice shell within a multi wall carbon nanotube are associated with the interfacial registry effects, registry barriers and the

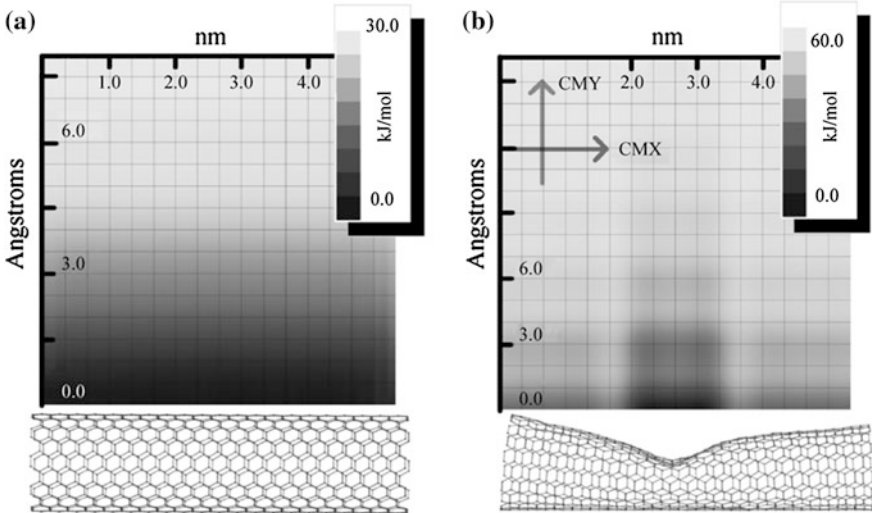


Fig. 8 A function representing the 2-D vdW energy (kJ/mol) varying with the distance from the outer surface for a (a) straight and (b) buckled single wall carbon nanotube (after [77])

accompanied generation of lattice waves, *phonons*, in the sliding carbon nanotube subjected to semi-constant force [12]. The onset of the interfacial registry between a carbon atom ‘asperity’ and a carbon ring potential barrier through a C–C bond is associated with the initiation of the so called *effect of the spatial exclusion of electrons (SEE)*⁶ in the repulsive interaction between the spatially-distributed π – π electrons [12]. After a carbon atom passes over a C–C bond and the thermodynamically unstable potential maximum, the C_{NT} lattice relaxes into and oscillates around a more favorable position within the potential well of a lattice-asperity registry under the ambient registry potential akin to the capillary effect. The local spatial energy map of π -electrons is affected by the transient interlocking of π -electrons, which is similar to the quasi-static interlocking illustrated by the energy map shown in Fig. 8b.

This sliding behavior of a carbon nanotube is also associated with the release of the lattice waves, i.e., *phonons* (see Fig. 9) [12] during sharp yet short peaks in the interfacial registry interlocking and the associated sharp but small drops in the C_{NT} sliding velocity, V_{NT} . This stick-slip phenomenon of the nanoscale friction is caused by the emergence of various registry-dependent interlocking of the atomic lattice barriers, which are sensitive and directly connected to the C_{NT} lattice sliding path,⁷ its carbon rings, as well as to the influence of lattice oscillations [12]:

Phonons in the Atomic Lattice Shells

At the nanoscale level, oscillations of the graphene lattice (Fig. 9) are inherent in most physical settings due to thermodynamic motion of carbon atoms. Lattice waves, i.e., *phonons*, in the atomic lattice structure of carbon nanotubes occur continuously due to the thermal vibrations, nanoscale mechanical deformation with complex loading path or complex sequence of thermodynamic equilibrium states (e.g., buckling [1, 8, 10–12, 48–54]) and during the tapping mode of the carbon

⁶ V.M. Harik, New Trends in Mechanics of Carbon Nanotubes and Applications, Technical Report TR-2012-2, Nanodesigns Consulting, Newark, Delaware, 2012.

⁷ Initiation of the so called *SEE effect* is associated with the need of at least one π -electron to overcome the registry potential of an opposing C–C bond and the associated Coulomb repulsion within the so called *spatial exclusion zone (SEZ)* for electrons. The size of the *spatial exclusion zone* depends on the local atomic lattice configuration (e.g., orientation of C–C bonds), the registry potential barriers, the nanoscale Coulomb repulsion proportional to $1/r^2$, and the nanoscale repulsion proportional to $-1/r^{12}$. The combined effect results in the so called *SEE effect*. The nanoscale analog of Pauli exclusion-repulsion for electrons stems from the quantum Pauli principle for the identical electrons, i.e. particles with the spin $1/2$ (*fermions*); the two identical particles cannot occupy the same energy state, as their combined wave function, ψ , is anti-symmetric. The nanoscale analog of Pauli repulsion and the quantum Pauli principle for the electrons both affect the precise dimensions of the spatial exclusion zone for interfacial electrons.

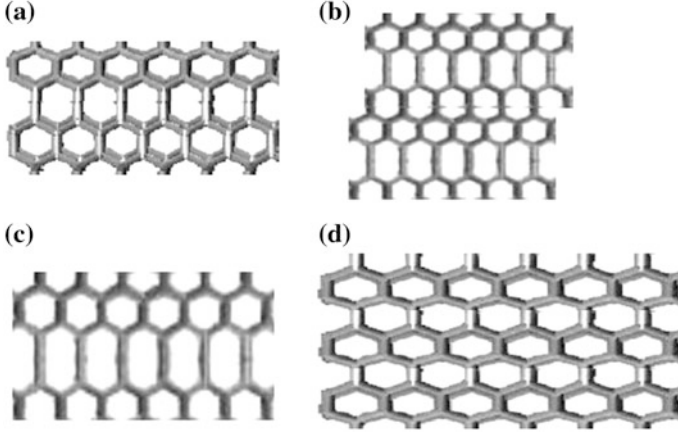


Fig. 9 Schematics of the longitudinal lattice waves (a), (b), (c) and (d) (i.e., longitudinal phonons) and tensile lattice deformations of the graphene sheets: local stretching (c) and the global or uniform tensile deformation (d)

nanotube based AFM probes (Fig. 5). Distribution of the low energy *border value (BV) phonons* of stochastic lattice waves [12] emerging at low temperatures in stochastic oscillations with the border value amplitudes depends on the energy of thermal vibrations. Probability and the dominant mode of these phonons are directly connected to the configuration of specific atomic lattice structures [12], for example, the curvature of atomic lattice in carbon nanotubes, Fig. 9 illustrates a few examples of *phonons* in a portion of graphene lattices of various sizes.

At the nanoscale level the generated lattice waves and the induced mechanical stresses, σ_{ij} , can produce various types of deformations (Fig. 9). The nanoscale mechanical stresses can be described by the following formula [39–41]:

$$\sigma_{ij,n} = -\frac{1}{\Lambda_n} \left(M_n V_{n,i} V_{n,j} + \sum_{m=1}^N F_{nm,i} r_{nm,j} \right), \quad (15)$$

where M_n is the mass of the n th-atom, Λ_n is the volume of the n th-atom, $V_{n,i}$ and $V_{n,j}$ are the i th and j th-components of the velocity vector of the n th-atom ($i, j = 1, 2$ and 3), $F_{nm,i}$ is the i th-component of the force interaction between the n th-atom and m th-atom (i.e., the inter-atomic potential gradient) and $r_{nm,j}$ is the j th-component of the difference between the position vectors of the n th-atom and m th-atom. Note that the velocity contributions to the values of thermodynamic stress components (15) include the intrinsic dynamic effects into the nanoscale mechanical stresses, containing the velocity-dependent thermal effects associated with *phonons*.



Fig. 10 The atomic force microscope (AFM) probe with the high aspect-ratio carbon nanotube tip (the orientation of the tip attachment is not completely vertical due to the orientation of the faces of the pyramidal tip)

Applications of Carbon Nanotubes

Since the discovery of carbon nanotubes in 1991 by S. Iijima and his lab,⁸ these fullerenes have become one of the most popular types of nanostructured materials and particles used in novel applications and studied by academic and industrial researchers⁹ and students. Examples of nanotube-based applications in nanotechnology include: *nanoscale probes, sensors and resonators, the atomic force microscope (AFM) probes* [48–54] (Fig. 10), *nanotube-enhanced polymer membranes and multifunctional nanocomposites* [12]. Carbon nanotubes or their fragments and graphene flakes are claimed to be found in women’s mascara, the fireplace ash, in the steel of Damascus swords, and soon to be found in advanced solar panels, fuel cells and batteries.

The Carbon Nanotube Based AFM Probes

Atomic force microscopes (AFM) are important instruments for the nanoscale characterization of material properties of various nanostructures, nanocrystals and molecules. Carbon nanotubes, both single wall carbon nanotubes and multi wall carbon nanotubes (Fig. 5) have been used as a high aspect ratio tip in the pyramidal AFM probes. Because of the smaller diameters ($\sim 1\text{--}2\text{ nm}$ and $\sim 50\text{--}70\text{ nm}$) of the available single wall and multi wall carbon nanotubes, respectively, resolution of the nanotube-based AFM probes is much higher as opposed to the pyramidal tip with diameters between 1 and 50 μm .

⁸ S. Iijima was awarded the 1996 Nobel Prize in Chemistry for “discovering fullerenes”, which also include carbon nanotubes.

⁹ V.M. Harik, *Mechanics of Carbon Nanotubes* © (2001), a short course, the Annual ASME Congress (2001, 2004) and the 2002 Nanosystems Conference (Berkeley, California).

Table 4 Typical length scales in the material structure of nanocomposites

Carbon nanotubes	Polymers	Polymer composites
Carbon ring (2.46 Å)	(CH ₂) zig-zag (~ 3 Å)	Fiber/matrix interphase (1–3 μm)
Diameter (~ 1 nm)	Crystalline unit (~ 7 Å)	Carbon fiber (20 μm)
Length (10 nm–cm)	Length of chains (~ 300 nm)	Fiber length (1–10 m)

AFM probes allow characterization of nanoscale surface profiles and the degree of roughness (Table 4), corrugation of atomic lattices, surface adhesion and friction, surface sliding and stiction, adhesion of single molecules and groups of atoms to the atomic lattices, the pullout and pull-off processes at the nanoscale, interfacial friction and atomic scale sliding or rolling of nanostructures, vibrational and material properties of carbon nanotubes (including nanoscale buckling [10–12, 50–52] [55–57]) as well as various manipulation processes [12, 48, 49] [48–54].

Carbon Nanotube Based Nanocomposites

Carbon nanotube based polymer nanocomposites [54–66] represent one of the highly promising multifunctional materials, which are sensitive to the electromagnetic field effects [12, 67, 68]. Typical length scales in the material structure of carbon nanotubes as compared to the polymeric structure of a crystalline polyethylene (PE) polymer (Fig. 11) and the polymer matrix composites reinforced by the carbon fibers [69, 70] are shown in Table 4. Carbon nanotube based *nanocomposites* or the nanotube-modified polymers have unique structural length scales, which are different from the hierarchical length scales associated with the microstructure of typical composites. One of the important characteristics of nanocomposites is the high ratio of interfacial surface to the volume of reinforcing carbon nanotubes or graphene flakes.

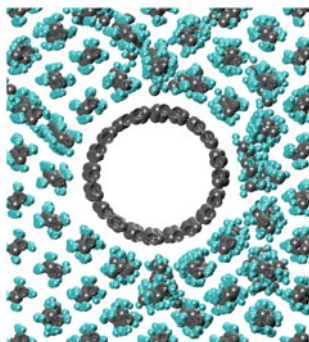


Fig. 11 Molecular lattice structure of the crystalline part of the polyethylene (PE) polymer with the (CH₂)_n zig-zag chains surrounding the armchair (10, 10) carbon nanotube, $d_{NT} = 13.6$ Å [78]

Another distinction of nanocomposites [53–66] is the small size of the representative volume element (RVE) or a unit cell (Fig. 11) in nanoscale homogenization [10–12, 39–41] or property averaging [12]. Intratubular space in carbon nanotubes contributes to their high porosity, however, it is not taken into account in the calculations of their volume fraction in nanocomposites. The C_{NT} volume fraction, V_{NT} , includes entire C_{NT} cross-section:

$$V_{NT} = \pi(R_{NT} + h_{NT}/2)^2/A_{RVE}$$

where $h_{NT} < h_{vdW}$ and h_{vdW} is the equilibrium van der Waals spacing between the C_{NT} lattice and the matrix, and A_{RVE} is the cross-sectional area of the unit cell. The value of effective C_{NT} thickness, h_{NT} , and the van der Waals separation distance, h_{vdW} , depend on the loading and the nature of the C_{NT} /polymer interfacial interactions. Therefore, the macroscopic volume fraction relation in micromechanics:

$$V_{NT} + V_m = 1$$

and Tsai's *rules of mixtures* [71] in micromechanics of composite materials for the longitudinal (E_1) and transverse (E_2) Young's moduli of a nanocomposite should be modified at nanoscale [12]:

$$V_{NT} + V_m = 1 - V_{vdW}, \quad (16a)$$

$$E_1 = E_{NT}V_{NT} + E_mV_m + E_{1int}V_{vdW}, \quad (16b)$$

$$\frac{1}{E_2} = \frac{V_{NT}}{E_{2NT}} + \frac{V_m}{E_m} + \frac{V_{vdW}}{E_{2int}}, \quad (16c)$$

so *the van der Waals volume fraction*, V_{vdW} , is included along with the matrix volume fraction, V_m , Young's moduli of the matrix, E_m , and the van der Waals interface, E_{int} , and some of the nanoscale effects (Table 5) are accounted for.

Material properties of nanotube-based nanocomposites depend on the structure-property relations and dependencies, which are different across the hierarchical length scales. In order to link a particular macroscopic material property with the nanoscale material characteristics or structural elements, an appropriate multi-scale “tree root” diagram is needed (Table 5). Dependence of the Young's modulus, E , on the material characteristics at different length scales is illustrated for the polymer composites based on the single wall and multi wall carbon nanotubes (SWNTs and MWNTs) and on traditional carbon fibers (Table 5).

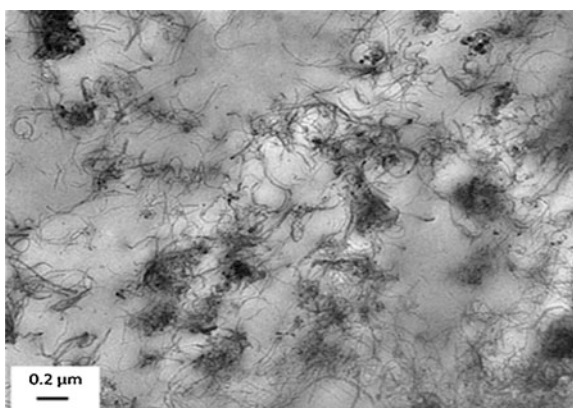
One of the first experiments characterizing the interfacial shear strength and the interfacial shear modulus has been carried out by Wagner and his group in 1998 [58–67, 71–73] by examining carbon nanotubes pulled out of a polymer matrix. Frankland et al. [39–41] carried out MD simulations to numerically evaluate the

Table 5 The structure-property relations for the Young's modulus in nanocomposites^a

The length scales	Nanocomposites	Polymer composites
Macroscopic	Entanglement, NT coil size	Volume fraction, E_m
Microscopic	NT bundles, clustering	Carbon fibers (size, E)
Submicron	SWNT versus MWNT effects	Interphase/interface
Nanoscale	NT/polymer interphase, polymer molecular weight	Crosslink density, interface structure
Atomic	NT/polymer bonding, molecular aromaticity	Polymer structure, molecular weight, etc.

^a The structure-property relations reflect the scale-based connections in the structure-property diagram, which links material properties with the material structure in the multiscale tree-root diagram for the structure-property relations [12]

Fig. 12 TEM image of a carbon nanotube polyethylene nanocomposite with 3.5 wt% of multi wall carbon nanotubes wrapped with 10 wt% of polyethylene-polyethylene oxide (after [79])



interfacial debonding force of about 0.1 nN between a carbon nanotube and polymer matrix in polyethylene nanocomposites. An example of a carbon nanotube based polyethylene nanocomposite is shown in Fig. 12.

Frankland and Harik [39–41] have confirmed earlier theoretical results for the critical debonding force, developed an MD-based modeling procedure to examine interfacial sliding of carbon nanotubes in the pull-out experiments and presented an interfacial friction model based on a nanoscale analog of the *Newton's friction law*. A nanoscale friction model [39–41], which is similar to the new interfacial model described by the Eq. (14), and the associated friction law have been used to simulate interfacial sliding of carbon nanotubes in a nanocomposite during a pull-out experiment. The axial displacement of a carbon nanotube and its sliding under an increasing axial force has been shown to be periodic as in the stick-slip processes [42, 74, 75] with the period of nanotube sliding equal to the size of carbon rings, a .

Conclusions

This chapter has presented a review of the basic models for carbon nanotubes in terms of the (n, m) nomenclature for the chirality of lattice structures and novel nanoscale effects such as *the effect of spatial exclusion of electrons (ESEE)*, which can be considered as a nanoscale analog of *the Pauli's exclusion principle* for electrons. An example of a spatial energy map for the spatially distributed π -electrons is included to illustrate a quasi-static spatial interlocking of the distributed π -electrons, which contributes to the viscosity of π -electrons. A nanoscale analog of the Newton's friction law has been introduced in a model for the interfacial friction between adjacent lattice shells in the multi walled carbon nanotubes involving a periodic stick-slip phenomenon.¹⁰ Interfacial lattice interlocking and the lattice registry effects also contribute to the effective viscosity of the spatially distributed π -electrons.

The ranges of applicability for different models for elastic deformation of carbon nanotubes within a particular class of carbon nanotubes have been discussed in the context of classification of their atomic lattices into *four classes (i.e., thin and thick lattice shells, long high-aspect-ratio nanotubes and beam-like carbon nanotube crystals of small radii)*. Applicability of different estimates for the effective thickness of carbon nanotubes varying between 0.66 Å (for axial buckling) and 3.4 Å (for transverse deformation dominated by van der Waals' forces) have been reviewed in the context of the balance between the elastic C–C bonds interactions and *van der Waals' forces*. The effect of van der Waals' interface in nanocomposites has been discussed for *the nanoscale rules of mixtures* and the nanotube/polymer interfacial sliding.

References

1. S. Iijima, Helical microtubules of graphitic carbon. *Nature*, **354**, 56 (1991) (Note that in 1991 S. Iijima has first referred to carbon nanotubes as 'microtubules' of graphitic carbon, which he and his colleague later changed to nanotubes in 1993 [2]. From the epistemological point of view this change from 'microtubules' to nanotubes indicates one of the first origins of the nanoscale concepts for new nanostructures, i.e., one of the first nanoparticles. Note that Buckminster ball, i.e., molecule C60, or the buckyball, was discovered in 1985 by R. Smalley.)
2. S. Iijima, T. Ichihashi, Single-shell (Note that in 1993 S. Iijima and T. Ichihashi have first proposed to consider carbon nanotubes as an atomic lattice 'shell'. The concept of a 'shell' was later used by B. Yakobson and his colleagues in their analysis of the carbon nanotube

¹⁰ In the late 15th century Leonardo da Vinci had identified the three important parts of friction as follows. "Friction is divided into three parts: these are simple, compound and disordered." Simple friction is due to the motion and dragging; the compound friction is "between two immovable things" and the irregular friction is associated with the "corners of different sides." For more details see the notebooks of Leonardo da Vinci [76].

- buckling [7, 8]. This was important from the epistemological point of view and for the development of new models for carbon nanotubes.) carbon nanotubes of low diameters. *Nature*, **363**, 603 (1993)
3. R.S. Ruoff, J. Tersoff, D.C. Lorents, S. Subramoney, B. Chan, Radial deformation of carbon nanotubes by van der Waals' forces. *Nature*, **364**, 514–516 (1993)
 4. J. Tersoff, R.S. Ruoff, Structural properties of a carbon nanotube crystal, (Note that in 1993 J. Tersoff and R. S. Ruoff have first recognized the importance of the carbon nanotube crystals (or bundles), which are important for the manufacturing of centimeter long carbon nanotubes based fibers more than fifteen years later.) *Phys. Rev. Lett.* **73**, 676 (1994)
 5. M.M.J. Treacy, T.W. Ebbesen, J.M. Gibson, Exceptionally high Young's modulus observed for individual carbon nanotubes. *Nature* **381**, 680 (1996)
 6. E.W. Wong, P.E. Sheehan, C.M. Lieber, Nanobeam mechanics: (Note that in 1997 C. Lieber and his colleagues have introduced the concept of nanobeams (as opposed to nanowires, for example) and an area in *Nanoscale Mechanics: Nanobeam Mechanics or Mechanics of Nanobeams*) elasticity, strength, and toughness of nanorods and nanotubes. *Science*, **277**, 1971 (1997)
 7. B.I. Yakobson, C.J. Brabec, J. Bernholc, Nanomechanics (Note that in 1996 B. Yakobson and his colleagues were among the first scientists, who have proposed to use a new term *Nanomechanics*, which has heralded the emerging field of *Nanoscale Mechanics*. They have also used the term "carbon tubes" for carbon nanotubes while they have utilized the concepts of macroscopic shell theory in the analysis of carbon nanotube buckling.) of carbon tubes: instabilities beyond linear response. *Phys. Rev. Lett.* **76**, 2511 (1996)
 8. B.I. Yakobson, T. Dimitrica, Chapter 1, in *Trends in Nanoscale Mechanics*, ed. by V.M. Harik, M. Salas (Kluwer Academic Publishers, Dordrecht, 2003), pp. 3–33
 9. R. Saito, M. Fujita, G. Dresselhaus, M.S. Dresselhaus, Electronic-structure of chiral graphene tubules. (Note that in 1992 (and 1991) the use of terms of "tubules" and "microtubules" for carbon nanotubes was present as an alternative term during the early stages of the emerging *Nanoscale Materials Science and Nanoscale Science of Nanostructured Materials*. The cited paper has also introduced the nomenclature for the physical description of carbon nanotubes and their chirality.) *Appl. Phys. Lett.* **60**, 18, 2204–2206 (1992)
 10. V.M. Harik, Ranges of applicability (Note that this paper was among the first addressing the ranges of applicability (and limitations) of continuum models to carbon nanotubes. Also note the criticism of the use of multiple macroscopic shells in the analysis of continuum cross-sectional area by S.J. Frankland, V.M. Harik, Analysis of carbon nanotube pull-out from a polymer matrix. *Mat. Res. Soc. Symp. Proc.* **733 E**, T6.2.1 (2002). In 1997 in their paper [13], B. I. Yakobson and R. Smalley expressed their hope that continuum mechanics can be applied at the level of "a few atoms", which was rather optimistic as was later demonstrated in the aforementioned papers.) for the continuum beam model in the mechanics of carbon nanotubes and nanorods. *Solid State Commun.* **120** (7–8), 331–335 (2001)
 11. V.M. Harik, Mechanics of carbon nanotubes: (Note that in 2001 [10], and in 2002, a particular area of *Nanoscale Mechanics: Mechanics of Carbon Nanotubes* was defined and its key basic concepts were outlined in a first nationally-distributed short course by V.M. Harik: *Mechanics of Carbon Nanotubes* © 2001 (a Short Course of ASME Education Institute, American Society of Mechanical Engineers (ASME), New York).) applicability of the continuum-beam models. *Comput. Mater. Sci.* **24**(3), 328–342 (2002)
 12. V.M. Harik, *Mechanics of Carbon Nanotubes* (Nanodesigns Press, Newark, 2011)
 13. X. Zhou, J.J. Zhou, Z.C. Ou-Yang, *Phys. Rev. B*, **62**, 13692 (2000)
 14. Z.C. Tu, Z.C. Ou-Yang, *Phys. Rev. B*, **65**, 233407–233414 (2002)
 15. A. Pantano, M.C. Boyce, D.M. Parks, *Phys. Rev. Lett.* **91**, 145504 (2004)
 16. A. Pantano, D.M. Parks, M.C. Boyce, *J. Mech. Phys. Solids* **52**, 789–821 (2004)
 17. S.V. Goupalov, *Phys. Rev. B*, **71**, 085420 (2005)
 18. P. Avouris, T. Hertel, R. Martel, T. Schmidt, H.R. Shea, R.E. Walkup, *Appl. Surf. Sci.* **141**, 20 (1999)
 19. T. Halicioglu, Stress calculations for carbon nanotubes. *Thin Solid Films*, **312**, 11 (1998)
 20. L. Wang, Q. Zheng, J.Z. Liu, Q. Jiang, *Phys. Rev. Lett.* **95**, 105501 (2005)

21. Y. Huang, J. Wu, K.C. Hwang, Phys. Rev. B, **74**(24), 24541 (2006)
22. K.N. Kudin, C.E. Scuseria, B.I. Yakobson, Phys. Rev. B, **64**, 235406 (2001)
23. A. Sears, R.C. Batra, Phys. Rev. B, **69**, 235406 (2004)
24. C.Q. Ru, Effective bending stiffness of carbon nanotubes. Phys. Rev. B, **62**(15), 9973 (2000)
25. S. Govindjee, J.L. Sackman, Solid State Commun. **110**, 227, 1999
26. S.P. Timoshenko, J.M. Gere, *Theory of Elastic Stability* (McGraw-Hill, New York, 1961)
27. M. Arroyo, T. Belytschko, J. Mech. Phys. Solids, **50**, 1941 (2002)
28. M. Arroyo, T. Belytschko, Mech. Mater. **35**(3–6), 193–215 (2003)
29. M. Arroyo, T. Belytschko, Phys. Rev. B, No. 69, Paper N 115415 (2004)
30. D. Stojkovic, P. Zhang, V.H. Crespi, Phys. Rev. Lett. **87**(12), 125502 (2001) (In 2001 V. H. Crespi [33] and his group at the Penn State University and V. M. Harik [34] at NASA Langley Research Center have independently predicted degeneration of C_{NT} lattice shells into nano-beams around the critical value of the normalized C_{NT} radius, $R_{NT}/a \approx 1$, Crespi predicted “breaking the symmetry of sp^3 bonds in tubular geometries” in the smallest nanotubes.)
31. V.M. Harik, *Ranges of Applicability for the Continuum-Beam Model in the Constitutive Analysis of Carbon Nanotubes: Nanotubes or Nano-beams?* NASA/CR-2001-211013, NASA Langley Research Center, Hampton, Virginia (2001)
32. B.I. Yakobson, R.E. Smalley, (In 1997 B.I. Yakobson and R. Smalley after a very successful paper on the origins of Nanomechanics [7, 8] have expressed rather optimistic hopes that the concepts of macroscopic continuum mechanics can be applied to nanostructures at the scale of “a few atoms”, which was later corrected by the nanoscale homogenization criterion as often happens in an emerging new science.) Am. Sci. **85**, 324 (1997)
33. C.Y. Li, T.-W. Chou, Int. J. Solids Struct. **40**, 2487–2499 (2003)
34. R.C. Batra, S.S. Gupta, ASME J. Appl. Mech. **75**, 061010 (2008)
35. A.N. Kolmogorov, V.H. Crespi, Phys. Rev. Lett. **85**(22), 4727 (2000)
36. K. Liao, S. Li, Appl. Phys. Lett. **79**(25), 4225 (2001)
37. A.N. Kolmogorov, V.H. Crespi, Phys. Rev. B **71**, 235415 (2005)
38. N. Marom, J. Bernstein, J. Garel, A. Tkatchenko, E. Joselevich, L. Kronik, O. Hod, Phys. Rev. Lett. **105**, 046801 (2010)
39. S.J.V. Frankland, V.M. Harik, Surf. Sci. Lett. **525**, L103 (2003)
40. S.J.V. Frankland, V.M. Harik, Mat. Res. Soc. Symp. Proc. **733** E, T6.2.1 (2002). (This research on the nanoscale friction modeling was supported in part by NASA and the Princeton University based NASA URETI Institute for the Bio-inspired Nanostructured Multifunctional Materials (see the Princeton University based web site: <http://bimat.org>, award No. NCC-1-02037 by the NASA Langley Research Center, Hampton, Virginia).)
41. S.J.V. Frankland, A. Caglar, D.W. Brenner, M. Griebel, J. Phys. Chem. B **106**(12), 3046–3048 (2002)
42. Q.Y. Li, K-S. Kim, Proc. R. Soc. A **464**, 1319 (2008)
43. M.S. Dresselhaus, P.C. Eklund, Adv. Phys. **49**(6), 705 (2000)
44. A.N. Cleland, *Foundations of Nanomechanics* (Springer, Berlin, 2003)
45. P. Tangney, M.L. Cohen, S.G. Louie, Phys. Rev. Lett. **97**(19), 195901 (2006)
46. X.H. Zhang, G.E. Santoro, U. Tartaglino, E. Tosatti, Phys. Rev. Lett. **102**(12), 125502 (2009)
47. V.M. Harik, R.A. Cairncross, Mech. Mater. **32**, 807 (2000)
48. M.F. Yu, B.I. Yakobson, R.S. Ruoff, J. Phys. Chem. **104**, 8764 (2000)
49. J. Buchoux, J.-P. Aime, R. Boisgard, C.V. Nguyen, L. Buchailot, S. Marsaudon, Nanotechnology **20**, 475701 (2009)
50. H. Dai, Nature **384**, 147 (1996)
51. K. Jensen, C. Girit, W. Mickelson, A. Zettl, Phys. Rev. Lett. **96** (21), 215503 (2006)
52. R. Stevens et al., Appl. Phys. Lett. **77**, 3453 (2000)
53. H. Nishijima, Appl. Phys. Lett. **74**, 4061 (1999)
54. J.H. Hafner, C.L. Cheung, T. Oosterkamp, C.M. Lieber, J. Phys. Chem. **105**, 743 (2001)
55. A. Garg, S.B. Sinnott, Chem. Phys. Lett. **295**, 273–278 (1998)
56. I.-L. Chang, B.-C. Chiang, J. Appl. Phys. **106**, 114313 (2009)

57. C.Y. Li, T.-W. Chou, *Mech. Mater.* **36**(11), 1047–1055 (2004)
58. L.S. Schadler, S.C. Giannaris, P.M. Ajayan, *Appl. Phys. Lett.* **73**, 3842 (1998)
59. S.B. Sinnott, O.A. Shenderova, C.T. White, D.W. Brenner, *Carbon*, **36**(1–2), 1–9 (1998)
60. H.D. Wagner, O. Lourie, Y. Feldman, R. Tenne, *Appl. Phys. Lett.* **72**, 188 (1998)
61. P.M. Ajayan, L.S. Schadler, S.C. Giannaris, A. Rubio, *Adv. Mater.* **12**, 750 (2000)
62. C.Y. Li, Chou, J. *Nanosci. Nanotechnol.* **3**(5), 423–430 (2000)
63. S.B. Sinnott, J. *Nanosci. Nanotechnol.* **2**(2), 113–123 (2002)
64. S.J.V. Frankland, V.M. Harik, G.M. Odegard, D.W. Brenner, T.S. Gates, *Compos. Sci. Technol.* **63**(11), 1655–1661 (2003)
65. Y. Hu, I. Jang, S.B. Sinnott, *Compos. Sci. Technol.* **63**(11), 1663–1669 (2003)
66. Z. Qunaies, C. Park, K.E. Wise, E.J. Siochi, J.S. Harrison, *Compos. Sci. Technol.* **63**(11), 1637–1646 (2003)
67. D. Srivastava, C. Wei, K. Cho, *Appl. Mech. Rev.* **56**(2), 215–230 (2003)
68. A.N. Cleland, M.L. Roukes, *Nature*, **320**, 160–161 (1998)
69. V.M. Harik, L.-S. Luo (eds.), *Micromechanics and Nanoscale Effects* (Kluwer Academic Publishers, The Netherlands, 2004)
70. T.W. Chou, *Microstructural Design of Fiber Composites* (Cambridge University Press, Cambridge, 1992)
71. E.T. Thostenson, C. Li, T.-W. Chou, *Compos. Sci. Tech.* **65**, 491–516 (2005)
72. R.C. Picu, A. Sarvestani, M.S. Ozmusul, Chapter 3, in V.M. Harik, M.D. Salas (eds.) *Trends in Nanoscale Mechanics* (Kluwer Academic Publishers, The Netherlands, 2003), pp. 61–87
73. Y. Hu, O.A. Shenderova, Z. Hu, C.W. Padgett, D.W. Brenner, *Rep. Prog. Phys.* **69**, 1847 (2006)
74. B.N.J. Persson, *Sliding Friction: Physical Principles and Applications* (Springer, Berlin, 1998)
75. B.N.J. Persson, *Surf. Sci. Reports* **33**, 83 (1999)
76. E. MacCurdy (ed.), *The Notebooks of Leonardo da Vinci* (Konecky and Konecky printing, Duckworth, London, 1906)
77. S. Gorantla, S. Avdoshenko, F. Börrnert, A. Bachmatiuk, M. Dimitrakopoulou, F. Schäffel, R. Schönfelder, J. Thomas, T. Gemming, J. H. Warner, G. Cuniberti, J. Eckert, B. Büchner, M. H. Rummeli, Enhanced π – π Interactions Between a C60 Fullerene and a Buckle Bend on a Double-Walled Carbon Nanotube. *Nano. Res.* **3**, 92–97 (2010)
78. S.J. Frankland, V.M. Harik, Analysis of carbon nanotube pull-out from a polymer matrix. *Mat. Res. Soc. Symp. Proc.* **733 E**, T6.2.1 (2002)
79. C. Semaan, G. Pecastaings, M. Schappacher, A. Soum, *Polym. Bull.* **68**, 465–481 (2012)
80. T. Vodenitcharova, L.C. Zhang, *Phys. Rev. B*, **68**, 165401 (2003)
81. M.-F. Yu, B.S. Files, S. Arepalli, R.S. Ruoff, *Phys. Rev. Lett.* **84**, 5552 (2000)

Trends in Nanoscale Mechanics

Mechanics of Carbon Nanotubes, Graphene,
Nanocomposites and Molecular Dynamics

Harik, V. (Ed.)

2014, XIII, 226 p. 126 illus., 40 illus. in color., Hardcover

ISBN: 978-94-017-9262-2